See related commentary on pg 2616

Autosomal Dominant Lamellar Ichthyosis Due to a Missense Variant in the Gene *NKPD1*

JID Open

Katalin Komlosi[1,2], Cristina Glocker[1,2], Hao-Hsiang Hsu-Rehder[1,2], Svenja Alter[1,2], Julia Kopp[1,2], Alrun Hotz[1,2], Andreas David Zimmer[1,2], Ingrid Hausser[3], Roger Sandhoff[4], Vinzenz Oji[5] and Judith Fischer[1,2]

The identification of monogenic causes for cornification disorders has enhanced our understanding of epidermal differentiation and skin barrier function. Autosomal dominant lamellar ichthyosis is a rare condition, and *ASPRV1* was the only gene linked to autosomal dominant lamellar ichthyosis to date. We identified a heterozygous variant (ENST00000686631.1:c.1372G>T, p.[Val458Phe]) in the *NKPD1* gene in 7 individuals from a 4-generation German pedigree with generalized lamellar ichthyosis by whole-exome sequencing. Segregation analysis confirmed its presence in affected individuals, resulting in a logarithm of the odds score of 3.31. *NKPD1* encodes the NKPD1 protein, implicated in the plasma membrane; its role in human disease is as yet unknown. Skin histology showed moderate acanthosis and compact orthohyperkeratosis, and the ultrastructure differed clearly from that in *ASPRV1*-autosomal dominant lamellar ichthyosis. Although *NKPD1* mRNA expression increased during keratinocyte differentiation, stratum corneum ceramides exhibited no significant changes. However, affected individuals showed an elevated ratio of protein-bound ceramides to omega-esterified ceramides. This highlights *NKPD1*'s role in autosomal dominant lamellar ichthyosis, impacting ceramide metabolism and skin lipid barrier formation, as demonstrated through functional characterization.

Keywords: Autosomal dominant lamellar ichthyosis, Mendelian cornification disorders, Nonsyndromic autosomal dominant congenital ichthyosis, NTPases, Whole-exome sequencing

Journal of Investigative Dermatology (2024) **144,** 2754–2763; doi:10.1016/j.jid.2024.03.041

INTRODUCTION

Ichthyoses comprise a broad spectrum of mostly inherited disorders characterized by generalized scaling, hyperkeratosis, and erythema, with or without associated extracutaneous manifestations (Fischer and Bourrat, 2020; Oji et al, 2010). The discovery of genetic causes of inherited keratinization disorders has greatly improved our understanding of epidermal differentiation. Several genes have been identified for autosomal recessive congenital ichthyosis (ARCI), and the specific forms are well-characterized (Fischer and Bourrat, 2020). More recently, pathogenic variants in *ASPRV1*, which encodes a stratified epithelium-specific protease important for FLG processing, have been shown to cause an autosomal dominant lamellar ichthyosis (ADLI) (Mendelian Inheritance in Man number 146750) (Boyden et al, 2020). ADLI was described clinically and histologically by Traupe et al (1984). A prominent transforming zone between the stratum granulosum and stratum corneum (SC) and lipid inclusions in the SC are characteristic ultrastructural features (Kolde et al, 1985). Recent genetic analysis of the family originally described by Traupe et al (1984) confirmed *ASPRV1*-associated ADLI (Boyden et al, 2020). ADLI must be distinguished from other autosomal dominant ichthyoses such as keratinopathic ichthyoses caused by variants in keratin genes (*KRT1*, *KRT2*, *KRT10*) and loricrin keratoderma caused by variants in the *LORICRIN* gene (Fischer and Bourrat, 2020; Hotz et al, 2016; Knöbel et al, 2015).

In this study, we report on the molecular basis of a distinct form of ADLI. The phenotype segregates in 4 generations of a family. All affected members investigated carry a missense variant in the *NKPD1* gene. *NKPD1* encodes for the NKPD1 protein and is predicted to be an integral component of the plasma membrane and have at least 2 transmembrane domains (Stelzer et al, 2016).

We present clinical, histological, ultrastructural, and genetic studies of this, to our knowledge, previously unreported gene defect and show the results of skin ceramide analysis by SC tape stripping. In addition, we generated 3-dimensional (3D) skin models to recapitulate the effect of the missense variant on epidermal differentiation.

[1]*Institute of Human Genetics, Medical Center, Faculty of Medicine, University of Freiburg, Freiburg, Germany;* [2]*Center for Cornification Disorders, Freiburg Center for Rare Diseases, Medical Center, University of Freiburg, Freiburg, Germany;* [3]*Institute of Pathology, Heidelberg University Hospital, Heidelberg, Germany;* [4]*Lipid Pathobiochemistry Group, German Cancer Research Center, Heidelberg, Germany; and* [5]*Department of Dermatology, University Hospital Münster, Münster, Germany*

Correspondence: Judith Fischer, Institute of Human Genetics, Medical Center, Faculty of Medicine, University of Freiburg, Breisacher Street 33, Freiburg 79106, Germany. E-mail: judith.fischer@uniklinik-freiburg.de

Abbreviations: 3D, 3-dimensional; ADLI, autosomal dominant lamellar ichthyosis; ARCI, autosomal recessive congenital ichthyosis; ESE, epidermal skin equivalent; FTSM, full-thickness skin model; K, keratin; POS-Cer, protein-bound ceramide fraction; SC, stratum corneum

Received 15 January 2024; revised 23 February 2024; accepted 8 March 2024; accepted manuscript published online 18 April 2024; corrected proof published online 25 May 2024

RESULTS

Phenotype of affected individuals

We present clinical and genetic data from 7 patients with a moderate form of ichthyosis from a large German pedigree showing an autosomal dominant mode of inheritance. Twelve individuals in 4 generations (Figure 1) showed a consistent skin phenotype (Figure 2a–e). Shortly after birth, all patients presented with mild ichthyosiform erythroderma predominantly affecting the trunk and the scalp. None presented with collodion membrane, and there were no complications during pregnancy or delivery. Lamellar scaling developed as fine, whitish scales on the trunk; arms; thighs; and scalp, whereas brownish–gray medium-sized scales were observed on the neck (Figure 2e), in the axillary region, on the lateral thorax (Figure 2d), and in inguinal areas. The erythema disappeared by adulthood in all individuals. As in lamellar ichthyosis, sweating ability was reduced but improved with age. Scaling improves with warmer temperatures, high humidity, and sweating but does not disappear completely. A very mild palmoplantar keratoderma and scaling on the back of the hand is present with palmoplantar hyperlinearity, very similar to ichthyosis vulgaris. Some individuals reported moderate pruritus. Moisturizers and keratolytics had a moderate effect on scaling. We suspected a yet unreported form of ichthyosis due to the clearly autosomal dominant inheritance in absence of *ASPRV1* variants and performed whole-exome sequencing in 3 affected individuals.

Identification of a missense variant in the *NKPD1* gene in all affected family members

Initial diagnostic panel sequencing of 66 cornification disorder–related genes revealed no pathogenic alterations in patient III/2. Whole-exome sequencing in patients III/2, IV/3, and IV/4 identified 44 shared heterozygous variants using stringent filtering (Supplementary Table S1). Using protein and RNA expression data (The Human Protein Atlas, 2023), 3 candidate genes associated with skin function or keratinization (*NKPD1*, *TMPRSS11E*, and *FGFBP1*) were identified. Segregation analysis in 4 affected and 3 unaffected family members showed that only the heterozygous variant ENST00000686631.1:c.1372G>T, p.(Val458Phe), chr19:g.45153065 (GRCh38.p13) in *NKPD1* cosegregated with the disorder, yielding a logarithm of the odds score of 3.31 (Figure 1) (Ott, 2001).

NKPD1 has 3 transcripts (ENST00000686631.1, ENST00000317951.6, and ENST00000589776.1). The variant affects all 3, with our nomenclature referring to the 4822 bp isoform ENST00000686631.1, where it is situated in exon 5 (Supplementary Figure S1). The c.1372G>T, p.(Val458Phe) variant is not listed in gnomAD (Genome Aggregation Database), version 4.0.0. Residue 458 is located within the Walker B motif, a highly conserved strand of the P-loop NTPase fold (Aravind et al, 2004).

Histopathological analysis of skin from affected family members

Histopathological analysis (H&E staining) of skin biopsies (III/1: aged 62 years, right lower abdominal wall; III/2: aged 60 years, left upper arm) showed a thickened SC escalating from ~8.1 mm in patient III/1 to ~28.4 mm in patient III/2 (Figure 3a–c). The skin biopsy from the inguinal region of patient IV/3 (aged 29 years) displayed moderate acanthosis, a regular basal and spinous layer, 1–2 layers of granular cells, and compact orthohyperkeratosis with follicular plugging (Figure 3d). No evidence of epidermolytic hyperkeratosis was found.

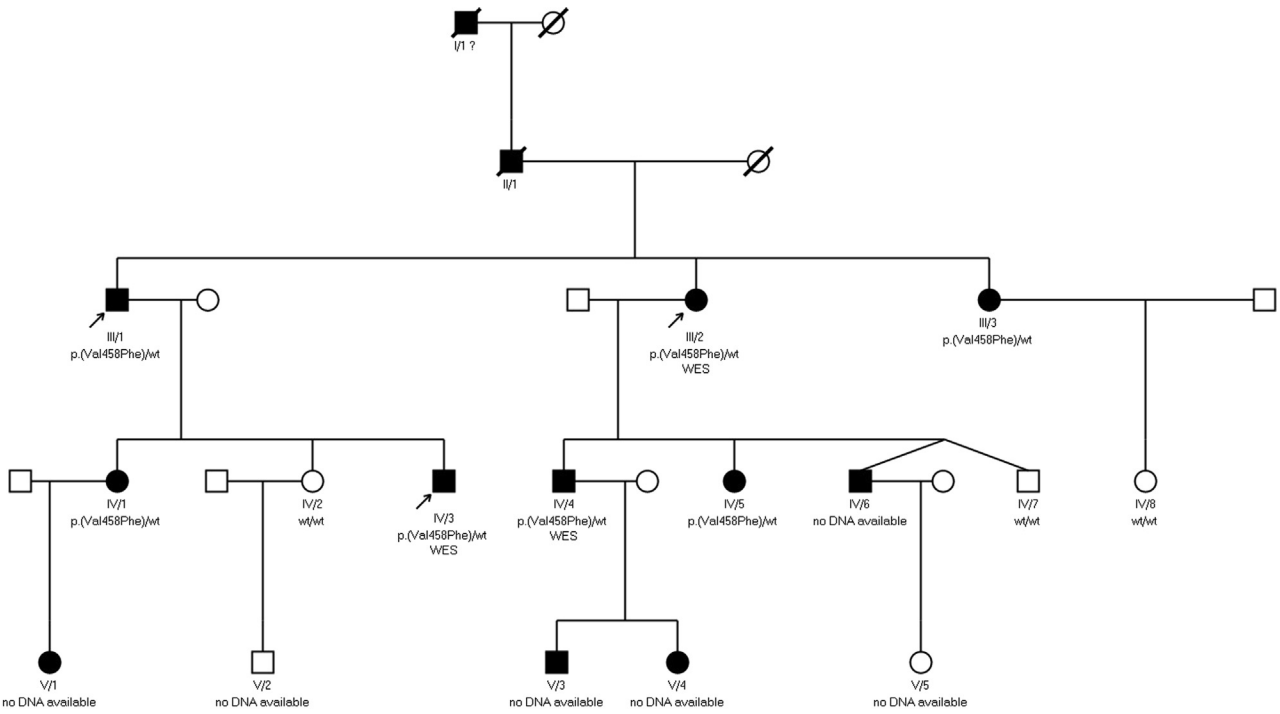

Figure 1. Pedigree of the family. Arrows indicate the 3 patients who underwent a skin biopsy and genotype data indicates a further 4 affected and 3 unaffected family members in whom segregation analyses were performed. The genotype is indicated for all analyzed family members. WES, whole-exome sequencing.

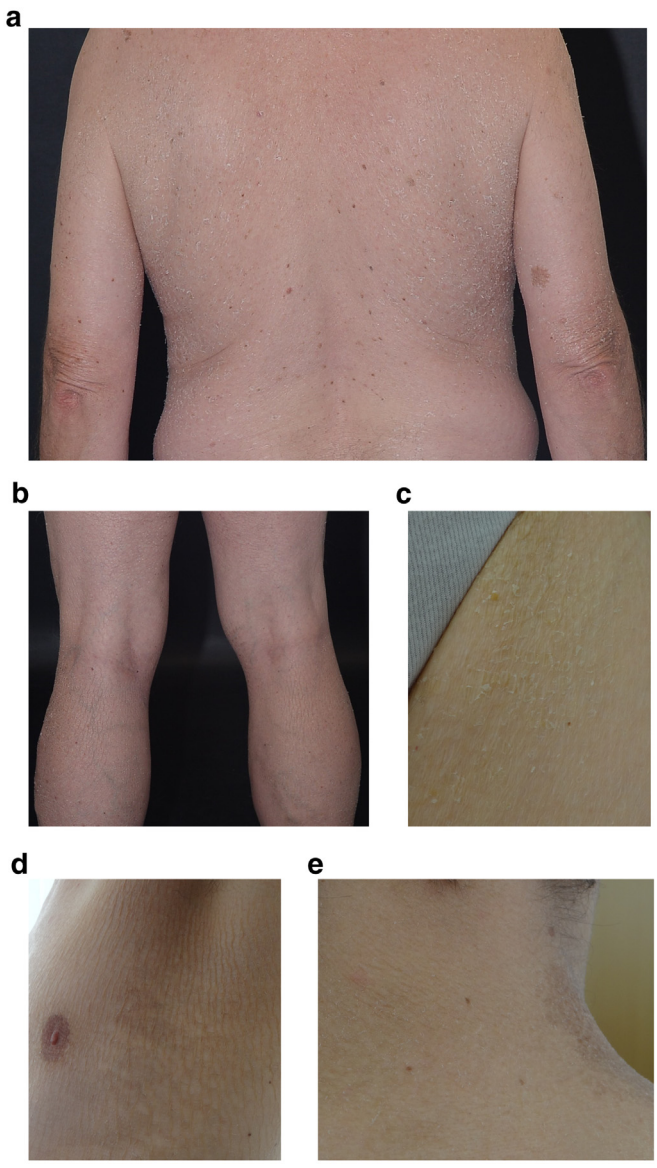

Figure 2. Skin manifestations in patients III/1, III/2, and IV/3. (**a, b**) All affected family members had mild generalized ichthyosis with very dry skin and scaling. Fine and white scales are observed in all individuals, most prominently on the trunk and on the upper arms, with sparing of the dorsal side of the knees. Medium-sized brownish–gray scales develop on the neck, axillary areas, and lateral thorax, especially in the younger affected family members (IV/3). (**d, e**) a: III/1. back; b: III/1. dorsal calves; c: III/2. left inguinal region; d: IV/3. lateral thorax and axillary region; e: IV/3. neck. All patients consented to the publication of their images.

Ultrastructural analysis

Electron microscopic examination of the skin biopsy from the upper left arm of patient III/2 at age 36 years (27 years ago) showed normal epidermal thickness, a thin granular layer (1–2 layers), reduced amounts of structurally unremarkable keratohyalin, and thin corneal lamellae (30–35 layers) with orthokeratosis. No cornified envelope aberrations were noted, and follicular plugging was evident. I. Anton-Lamprecht was able differentiate the ultrastructural features between 2 German families with ADLI—the first family described by Traupe et al (1984) and Kolde et al (1985) and the second family presented in this study—although the genetic background in those families was not known at that time. Whereas electron microscopic analysis in the *ASPRV1*-associated ADLI family showed a prominent transforming zone between the stratum granulosum and SC, a normal keratin pattern, and only a limited number of SC lipid inclusions, in the family (III/2) described in our study, normal epidermal thickness, absence of hyperproliferation, and absence of specific lipid inclusions in the SC were seen.

Recent ultrastructural analysis of a skin biopsy of patient IV/3 showed no systematic aberrations of terminal differentiation or keratinization. The SC had 40–60 layers of mostly homogeneous flat horny lamellae, a regular keratin pattern, and no inclusions. The stratum granulosum had 1–3 layers with normal keratohyalin granules, lamellar bodies, and tonofilaments (Supplementary Figure S2). Overall, there was no specific ultrastructural marker for a known keratinization disorder. The mild changes seen in patient IV/3 align with previous analyses (III/2) and differ from features of known keratinization disorders, such as ARCI, ichthyosis vulgaris, or *ASPRV1*-associated ADLI.

Immunohistochemistry and immunofluorescence analysis

To assess the impact of the *NKPD1* missense variant on protein expression and epidermal differentiation markers, we conducted immunostaining on skin biopsy from patients III/1, III/2, and IV/3 with antibodies against NKPD1, cytokeratin 6, cytokeratin 1/10, involucrin, FLG, and glucosylceramide. NKPD1 was expressed from the basal to the granular epidermal layers. In the control, the expression showed a concentration gradient with increasing NKPD1 from basal to suprabasal layers. Immunostaining in the patients was more intense, with the same intensity throughout all the layers (Figure 3e–h). Immunolocalization of cytokeratin 6 showed restriction to the basal layer in patients and control, and cytokeratin 1/10 was localized in the suprabasal layers in both. However, the demarcation of the basal layer by cytokeratin 6 and cytokeratin 1/10 was less distinct in patients III/1, III/2, and IV/3, with staining extending across several layers (Figure 3r–t), especially in III/2 and IV/3. FLG and involucrin immunostaining revealed no significant differences between patients and controls (Figure 3i–p). In control skin, glucosylceramide was prominent in the stratum granulosum. At the edge of the SC, the fluorescence was very strong and decreased toward the basal layer (Figure 3u). Patients III/1, III/2, and IV/3 exhibited reduced glucosylceramide staining compared with the healthy control (Figure 3v–x).

The 3D skin models from patient keratinocytes

Previously, we successfully applied skin models to study ARCI (Heinz et al, 2017). Owing to limited patient samples, we reduced the skin model size to a 24-well format. Two approaches were explored: an epidermal skin equivalent (ESE) (Figure 4a and c), following Thermo Fisher Scientific's published instruction, and a full-thickness skin model (FTSM) (Figure 4b and d), optimized from Schimek et al (2018). The FTSM better replicated skin layer thickness and hyperkeratosis than the ESE, using keratinocytes from patient III/1 and a healthy control.

All the models produced had 4–5 layers of living keratinocytes on day 14, with clearer distinction in the FTSM than in the ESE (Figure 4). The FTSM SC of patient III/1 (Figure 4d)

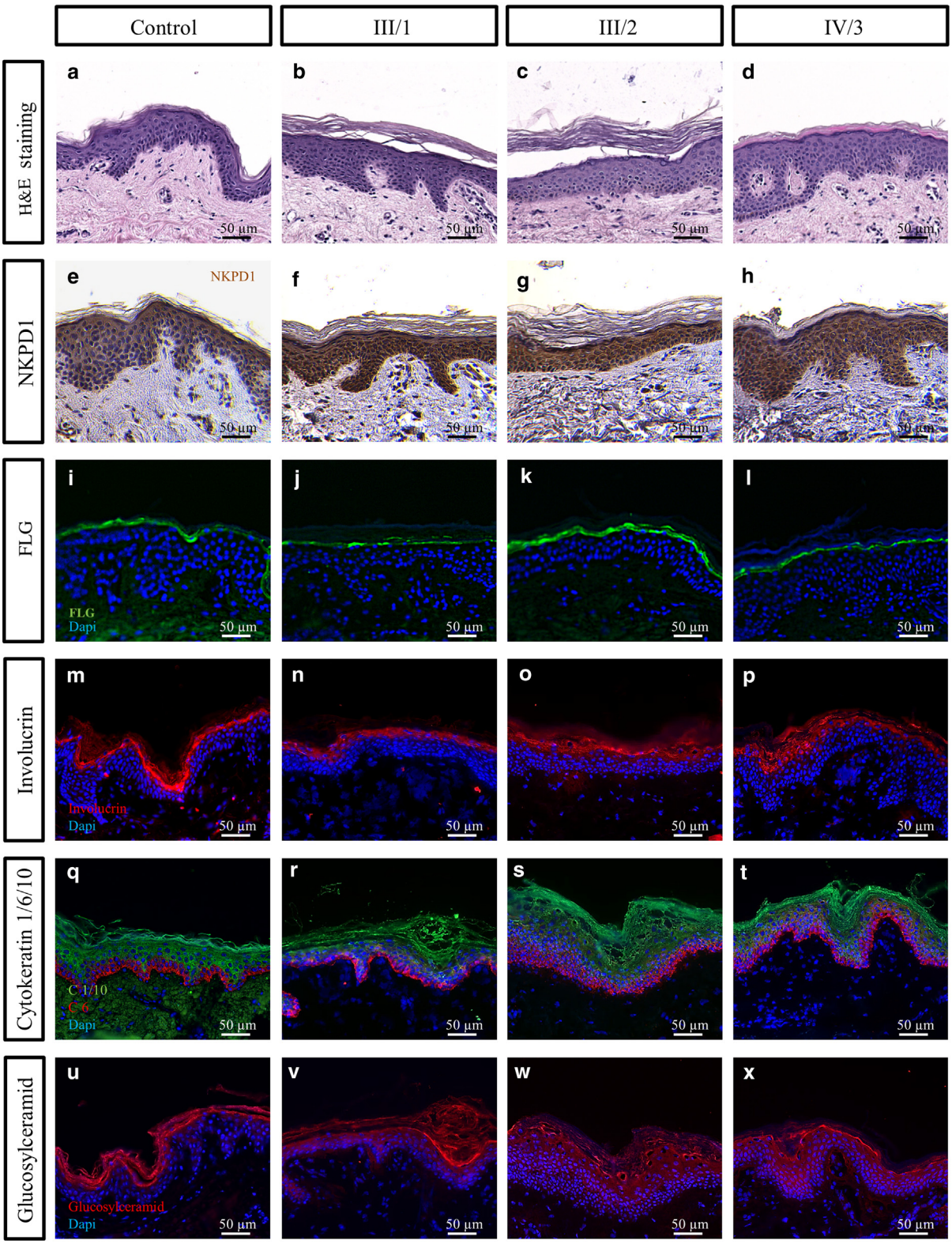

Figure 3. Skin histology, immunohistochemistry, and immunofluorescence analysis of patients III/1, III/2, and IV/3 and a healthy donor. (**a**–**d**) H&E staining of patients shows thicker stratum corneum (III/1 and III/2) and acanthosis (IV/3) than of a healthy control. (**e**–**h**) The brownish staining in immunohistochemistry shows the expression of NKPD1 in the epidermis. (**i**–**x**) Immunofluorescence staining of the skin of all affected family members; cytokeratin 1/10 is expressed more in the stratum granulosum than in the stratum spinosum, and glucosylceramide seems to be reduced. There is no significant difference in the expression of FLG and involucrin between skin samples from patients and healthy controls.

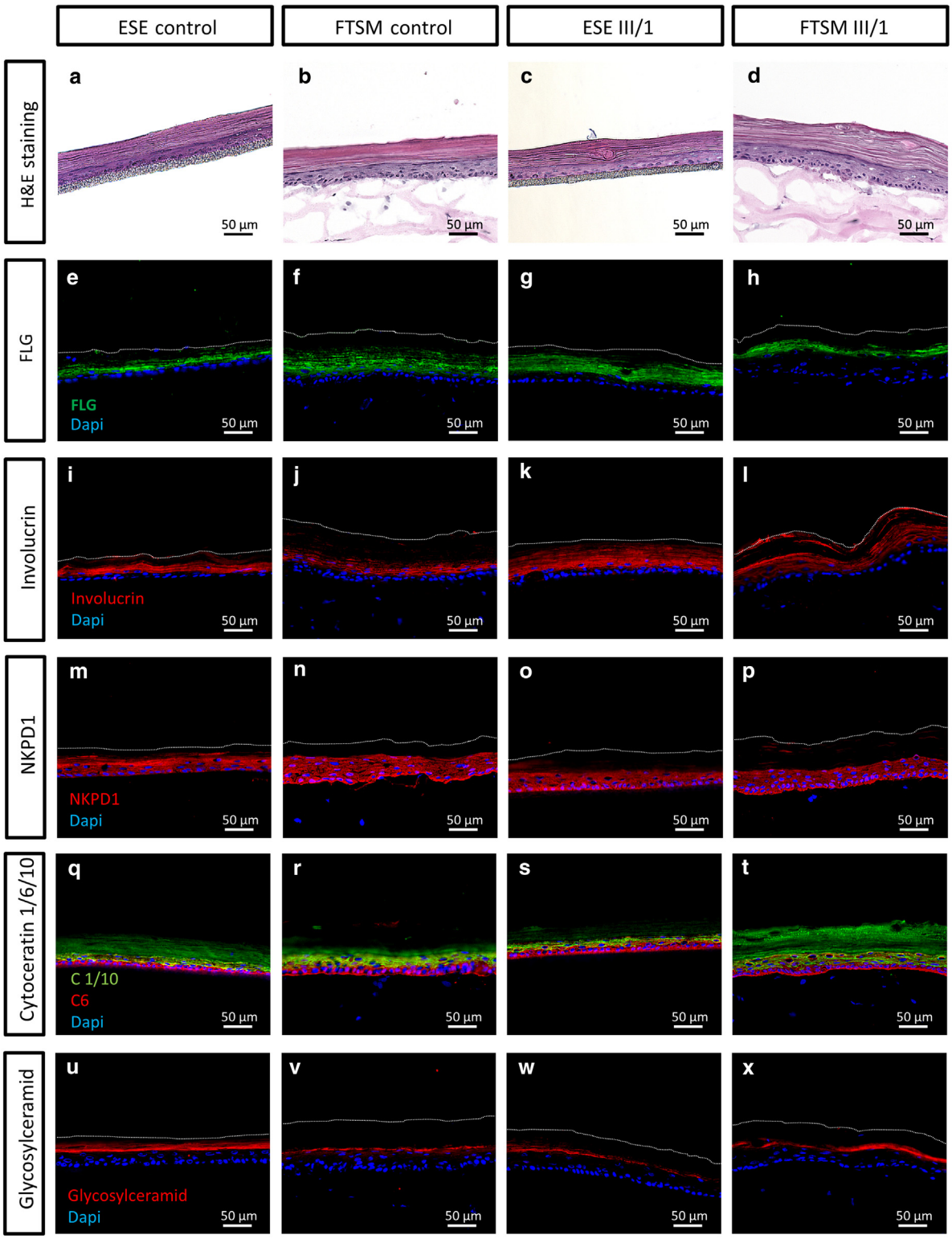

Figure 4. Histological and immunofluorescence analysis of skin models. (**a**–**d**) H&E staining of the skin models shows hyperkeratosis with orthokeratosis in the stratum corneum of patient III/1. (**e**–**x**) Immunofluorescence staining visualizing the physiological development of the skin models. FLG, involucrin, and glucosylcermid are expressed in the stratum spinosum to stratum granulosum. Counterstaining with cytokeratin 1/10 (green) and cytokeratin 6 (red) shows the stratum basale. NKPD1 is expressed in the stratum basale to stratum granulosum. The dashed line indicates the edge of the stratum corneum. ESE, epidermal skin equivalent; FTSM, full-thickness skin model.

was thicker (~51.4 ± 5.8 μm, n = 3) than that of the control (~35.5 ± 1.7 μm, n = 3) (Figure 4b), indicating hyperkeratosis with orthokeratosis. H&E-stained sections of patient FTSM revealed interspersed dyskeratotic horny keratinocytes. The difference in SC thickness between control (~35.6 ± 4.7 μm, n = 3) and patient (33.3 ± 1.7 μm, n = 3) was less pronounced in the ESE models (Figure 4a and c).

FLG and involucrin are both expressed in the stratum spinosum to stratum granulosum of the skin models (Figure 4e–l). Combined staining for cytokeratin 1/10 and cytokeratin 6 visualized the stratum basale, revealing a transitional monolayer (Figure 4r and t).

The *NKPD1* variant affects mRNA expression in patients' skin

Because there is no information about the function of *NKPD1* in human keratinocytes, we first tested its expression pattern in RNA from keratinocytes. *NKPD1* transcripts ENST00000317951.6 and ENST00000589776.1 were separately detectable by RT-PCR in RNA extracted from keratinocytes of both healthy controls and patients. Expression of both transcripts was also detected in RNA from fibroblasts and leukocytes; a reduced expression of *NKPD1* in fibroblasts compared with that in keratinocytes was confirmed by qPCR (Supplementary Figure S3b). However, because most of the sequences of the 2 long transcripts overlap, and the unique part for ENST00000686631.1 is very short, we were unable to design primers to detect expression of this isoform separately.

Monitoring the relative expression of *NKPD1* mRNA during keratinocyte differentiation in in vitro 2-dimensional culture showed that its expression increased over time, reaching highest levels on day 14 of culture. Pooled results of 2 independent differentiation experiments are shown in Figure 5. Relative expression of *NKPD1* increased significantly more over time in the keratinocytes from the affected individual than in those from the healthy donor in both experiments.

Increased protein-bound ceramide fraction in patients' skin

On the basis of data from the functional prediction tool GeneNetwork, Amin et al (2017) suggested *NKPD1*'s involvement in the sphingolipid de novo synthesis, although, no functional data were provided. On the basis of this assumption, we explored sphingolipid metabolism in the skin of affected individuals from the family involved in this study. Lipid extraction from tape-stripped SC layers of the forearms revealed no significant ceramide synthesis defect in the patients (III/1, III/2, and IV/3) compared with that in age-matched controls. However, ultraperformance liquid chromatography electrospray ionization tandem mass spectrometry analysis (according to Pilz et al [2022]) showed a 2.5-fold increase in the protein-bound ceramide fraction (POS-Cer) in patient samples, leading to a significant relative rise in the ratio of protein-bound ceramides to omega-esterified ceramides (Figure 6).

DISCUSSION

ADLI was first described as a new entity by Traupe et al (1984) in a German family spanning several generations. Many years later, the molecular genetic background involving the German family was elucidated, and this subgroup of lamellar ichthyosis could be classified as *ASPRV1*-associated ADLI (Boyden et al, 2020). In this study, we report a distinctive form of ADLI in another large German pedigree with 12 affected individuals over 4 generations (Figure 1) caused by a missense variant in the previously unreported disease gene *NKPD1*. All affected members exhibited a consistent skin phenotype (Figure 2) that differed from that seen in *ASPRV1*-associated ADLI. In *ASPRV1*-associated ADLI, erythema is absent or mild, whereas

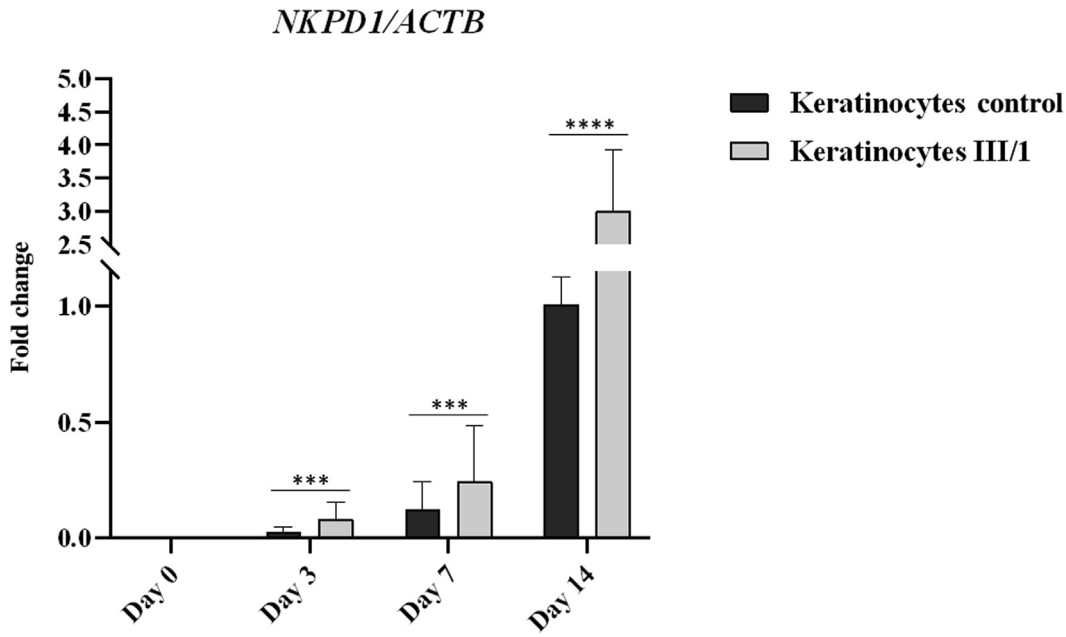

Figure 5. *NKPD1* expression in keratinocytes from patient III/1 and a healthy donor and during 2D differentiation. Relative *NKPD1* mRNA expression after 2D differentiation is shown. Pooled results from 2 independent differentiation experiments are shown. Data were normalized to the mean relative expression in keratinocytes from a healthy control on day 14 of differentiation. 2D, 2-dimensional.

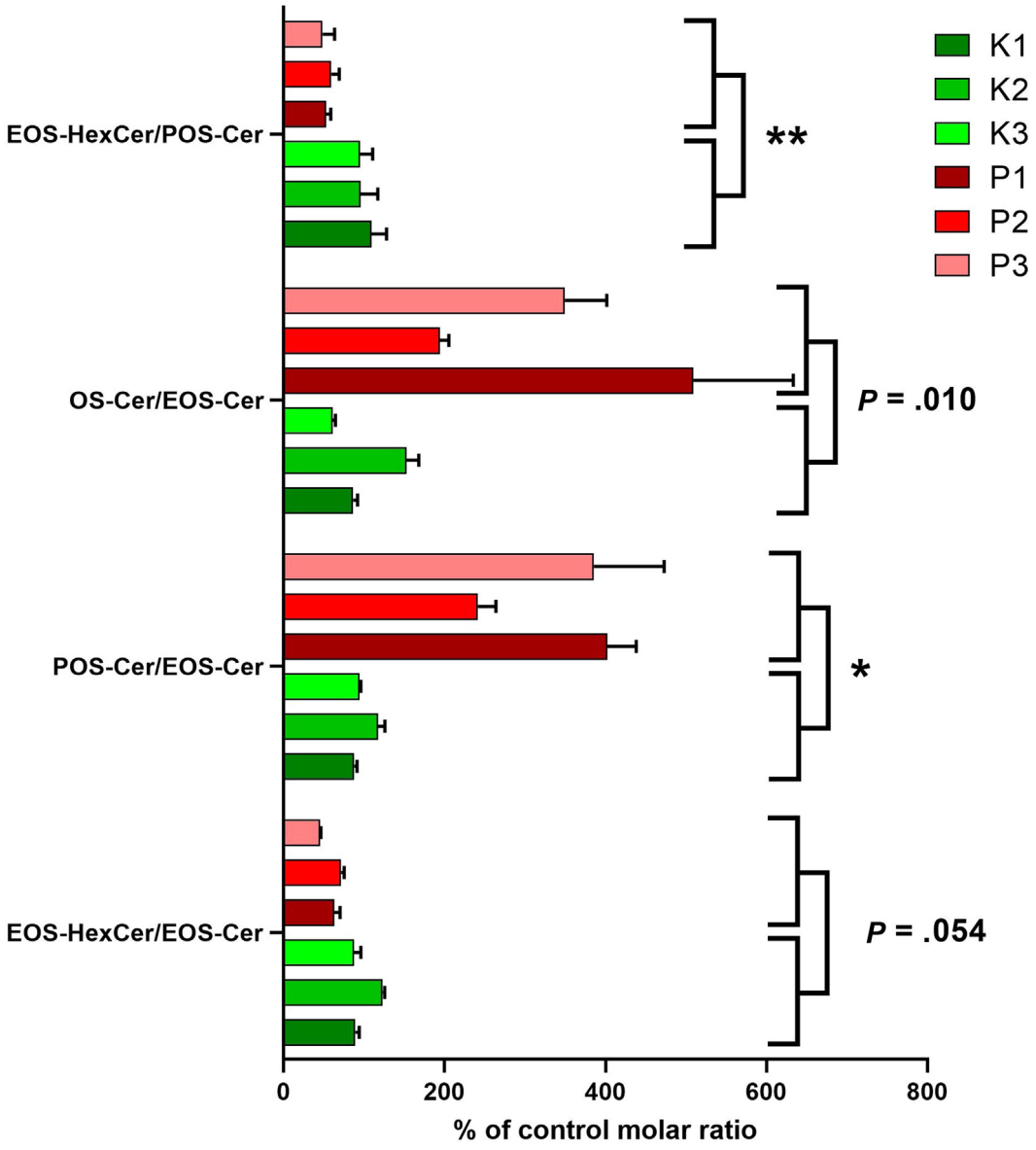

Figure 6. Ratio of esterified and protein-bound ceramides in patients and controls. Ceramides and hexosylceramides (presumably glucosylceramides) were quantified from stratum corneum samples of patients and controls by liquid chromatography–coupled tandem mass spectrometry as described in the Supplementary Material and Methods and converted to molar ratios. OS-Cer denotes ceramides containing an ultralong omega-hydroxy acyl chain and a sphingosine, EOS-Cer denotes OS-Cer with linoleic acid esterified to the omega-hydroxy group, POS-Cer denotes OS-Cer bound to proteins either through the omega-hydroxy group or through the modified linoleic acid residue, and EOS-HexCer are EOS-Cer with a hexosyl head group in the 1-O-position of the sphingoid base. The hexosyl residue is likely to be a glucosyl moiety. EOS-HexCer is precursor of lamellar EOS-Cer and of POS-Cer. EOS-Cer, omega-esterified ceramide; POS-Cer, protein-bound ceramide fraction.

in *NKPD1*-associated ADLI, there is always mild ichthyosiform erythroderma at birth and in childhood, which disappeared in all affected adults. In contrast to the large and plate-like dark brown scales over the entire body in *ASPRV1*-associated ADLI (Boyden et al, 2020; Traupe et al, 1984), lamellar scaling in *NKPD1*-associated ADLI develops as fine, whitish scales on the trunk (Figure 2a); arms; thighs; and scalp, with brownish–gray to whitish, medium-sized scales observed on the neck (Figure 2e), lateral thorax (Figure 2d), axillary, and inguinal areas. Overall, the disease expression in the family involved in this study appears to be more pronounced than in ichthyosis vulgaris but less severe than in *ASPRV1*-associated ADLI.

The term lamellar ichthyosis is not used in a standardized way and varies according to country or experience in the field of ichthyosis. According to the new terminology of lamellar ichthyosis introduced by Frost and van Scott (1966), lamellar ichthyosis is characterized as hyperproliferative hyperkeratosis. In Traupe's book "The Ichthyoses" from 1989, the term lamellar ichthyosis is used for all nonbullous (nonepidermolytic) and isolated forms of congenital ichthyoses (Traupe, 1989). In the patients from the family presented in this study, we observed both intrafamilial and intraindividual variability in the appearance and severity of the scaling that, in our opinion, would most likely be classified as lamellar ichthyosis. External factors, such as the

season, temperature, and humidity, had an influence on the phenotype.

Skin histology in 3 affected members of our family showed a thickened SC, moderate acanthosis, and compact orthohyperkeratosis with follicular plugging (Figure 3b–d). We did not observe an extended granular layer with coarse keratohyalin granules, and the ultrastructural analysis did not show a prominent transforming zone between the stratum granulosum and SC as described in *ASPRV1*-associated ADLI (Kolde et al, 1985). In our patients, no systematic ultrastructural aberrations of components involved in terminal differentiation and keratinization were observed, and no specific ultrastructural marker for a known keratinization disorder was found. However, the mild alterations significantly differed from the electron microscopic features of ARCI, ichthyosis vulgaris, or *ASPRV1*-associated ADLI.

Functional analysis in *ASPRV1*-associated ADLI confirmed impaired FLG processing (Boyden et al, 2020). The role of *NKPD1* in human physiology and, in particular, the cornification cycle is not yet known. *NKPD1* encodes the NTPase KAP Family P-Loop Domain-Containing Protein 1 (NKPD1) protein and is a member of the KAP family of P-loop NTPases (Aravind et al, 2004). P-loop NTPases form 1 of the major superfamilies that mediate a variety of cellular processes, including mRNA translation, signal transduction, cell motility, and growth regulation (Balasingam et al, 2020). Most of the P-loop domains are characterized by 2 conserved motifs—the Walker A and B motifs—which are responsible for the NTPase activity of the protein (Supplementary Figure S3b). However, sequence alignments of the KAP family NTPases suggest that the NTPase domain of NKPD1 is disrupted and may therefore have a function other than NTPase activity (Aravind et al, 2004).

NKPD1 was found to be highly expressed in the skin (expression data from Ensembl) and to a lesser extent in cerebellum, other brain tissues, and thyroid (GeneCards, 2023; Stelzer et al, 2016). There are no data on the role of NKPD1 in keratinocyte differentiation, nor are the targets or precise interaction partners known. According to Gene Network predictions, *NKPD1* is involved in several pathways, for example, cornified envelope formation and sphingolipid metabolism. Interaction partners include known ARCI genes (*SDR9C7*, *CERS3*) and genes involved in cornification disorders (*KRT1*, *KRT2*, desmoglein 1 gene *DSG1*).

Immunohistochemical analysis showed increased and continuous expression of NKPD1 in all layers of the epidermis in the patients. Whereas in the control, a concentration gradient from basal to suprabasal was evident, in patients, the expression showed the same intensity in all layers, starting with an increased expression already in the basal keratinocytes (Figure 3e–h). This may point to an aberrant regulation of NKPD1 in patients. There was no significant change in FLG expression (Figure 3i–l). In the 3D skin models generated with patient keratinocytes, the immunofluorescence staining showed a regular development of all skin models and no changes in the expression of NKPD1, cytokeratin 6, cytokeratins 1 and 10, FLG, involucrin, and glucosylceramide (Figure 4e–x). *NKPD1* mRNA expression in patients' undifferentiated keratinocytes and fibroblasts was comparable with *NKPD1* mRNA expression in the healthy controls. During keratinocyte differentiation in in vitro 2-dimensional culture, the highest levels of expression were reached on day 14, suggesting a role for NKPD1 in the outer layers of the epidermis (Figure 5). The increase in expression was significantly higher in patients' keratinocytes than in control keratinocytes up to day 14 of culture, suggesting compensatory gene expression in patients triggered by possible altered protein function. Another possibility would be that the point variant might create new binding sites for transcriptional activators or remove binding sites for repressors, resulting in an overall increase in the transcriptional activity of the gene.

Because *NKPD1* has been proposed to be involved in sphingolipid metabolism, we analyzed skin ceramides in topographically different compartments of the epidermis. Immunofluorescence analysis of the skin biopsies from patients assessed showed slightly reduced glucosylceramide levels in the stratum granulosum to stratum basale (Figure 3v–x). Using skin tape stripping, ceramides from the upper 8–10 layers of the SC of the affected patients were analyzed. In the lipid pattern of plantar scales from patients with ADLI described in 1984, Melnik et al (1989) found a marked alteration characterized by excessive amounts of free fatty acids and triglycerides, increased n-alkanes, reduced free sterols, and decreased total ceramides. Analysis of ceramide species on native SC from our patients showed no significant changes in skin ceramides, with no evidence of a synthesis defect. However, we observed a significant increase (2.5 fold) in the POS-Cer in the patient samples compared with that in age-matched controls (Figure 6). This may suggest a role for *NKPD1* in the POS-Cer biosynthesis pathway. One explanation for the increased POS-Cer could be that the missense variant in *NKPD1* leads to altered protein–protein interaction, affecting the proteins of the cornified envelope to which protein-bound ceramides are covalently bound (Akiyama, 2017; Candi et al, 2005). Involucrin has been identified as the major binding target protein of POS-Cer, but desmoplakin, envoplakin, periplakin, and loricrin have also been reported to bind to POS-Cer (Jennemann et al, 2012; Marekov and Steinert, 1998). Immunofluorescence analysis did not reveal altered expression of involucrin, but the influence of other target proteins cannot be excluded.

The increased POS-Cer fraction may also be an indirect consequence of the *NKPD1* missense variant because protein-bound ceramides are specifically enriched in the newly formed SC lamellae, and the proportion of the latter may be increased in cornification disorders, with potentially delayed degradation of protein-bound ceramides by acid ceramidase in these patients. However, no increase in esterified ceramides or in the degradation product of the protein-bound ceramides and fatty acids was seen, indicating that the delayed degradation of protein-bound ceramides does not sufficiently explain the observed increase in the ratio of protein-bound ceramides to omega-esterified ceramides (ie, POS-Cer/omega-esterified ceramides).

Our study suggests a yet unreported role for NTPases in skin homeostasis and possibly in epidermal differentiation. We show that the clinicogenetic spectrum of ADLI should be expanded and that a missense variant of the *NKDPD1* gene adds a distinctive form to the list of nonsyndromic dominant

congenital ichthyoses. Because the only alteration observed was a significant increase (2.5 fold) in the POS-Cer, a role for *NKPD1* in skin ceramide metabolism cannot be excluded. No monogenic human disease has been associated with variants in *NKPD1* so far. The discovery of patients with an ichthyosis phenotype as described in our study should promote routine analysis of *NKPD1* in patients with ARCI/ADLI as well as ichthyosis vulgaris. We can therefore now only speculate whether the *NKPD1* variants represent a genotype with a very low prevalence or whether the associated disease is simply underdiagnosed clinically owing to its overlap with ichthyosis vulgaris and mild forms of ARCI.

MATERIALS AND METHODS

Whole-exome sequencing and Sanger sequencing

Genomic DNA was isolated from peripheral blood samples from 7 affected and 3 unaffected family members. A gene panel of 66 genes associated with nonsyndromic and syndromic ichthyosis was initially performed on DNA from patient III/2. For further analysis, whole-exome sequencing of the index patient (III/2), her son (IV/4), and her affected nephew (IV/3) was performed. Candidate causative variants were validated, and segregation analyses in affected and unaffected family members were performed by Sanger sequencing. Detailed technical information is provided in the Supplementary Materials and Methods.

Human skin sample collection

A healthy skin sample from a female patient aged 34 years was obtained from leftover skin collected during excisional surgery. Skin biopsies were obtained from patients III/1, III/2, and IV/3 (Figure 1). Detailed protocols for isolation of primary keratinocytes and fibroblasts from skin biopsies, H&E staining, immunohistochemical/immunofluorescence staining, electron microscopic analysis, RNA analysis, and mass spectrometric ceramide analysis are provided in Supplementary Materials and Methods.

The 2-dimensional differentiation of keratinocytes

The 2-dimensional differentiation was performed on primary keratinocytes isolated from skin biopsies of patient III/1 and a healthy donor. Cells were cultured in EpiLife medium (Thermo Fisher Scientific) containing 1% human keratinocyte growth supplement (Thermo Fisher Scientific). Differentiation was induced by the addition of 1.1 mM calcium chloride, 0.03 mM palmitic acid (Sigma-Aldrich), and 0.015 mM linoleic acid (Sigma-Aldrich). A control group without calcium chloride was cultured simultaneously. The differentiation process was monitored over 14 days at 4 different time points (days 0, 4, 7, and 14).

Generation of 3D skin models

Two different 3D skin models, ESEs and full-thickness skin equivalents, were generated using primary keratinocytes from patient III/1 and a healthy donor. The ESEs were established according to the protocol by Thermo Fisher Scientific (Scott et al, 2016). Full-thickness skin equivalent generation was based on our previously published protocol (Schimek et al, 2018), optimized, and adapted to 24-well Nunc cell culture inserts (0.4 μl pore size) (Thermo Fisher Scientific). Detailed protocols are provided in the Supplementary Materials and Methods.

Statistical analysis

Data were analyzed with the Prism GraphPad software program, version 10.0.2, using nonparametric Mann–Whitney tests. Differences were considered significant at $P < .05$. Logarithm of the odds scores were calculated, and the significance metric thresholds were used according to Lander and Kruglyak: suggestive, logarithm of the odds ≥ 1.9; significant, logarithm of the odds ≥ 3.3 (Lander and Kruglyak, 1995).

ETHICS STATEMENT

Sample collection was approved by the Institutional Review Board of the University of Freiburg (reference number 436/17). Written informed consent was obtained from all patients, and all patients consented to the publication of their images. This study was conducted in accordance with the principles of the Declaration of Helsinki.

DATA AVAILABILITY STATEMENT

All relevant data generated or analyzed during this study are included in this published article. The complete datasets used and/or analyzed during this study are available from the corresponding author upon request.

ORCIDs

Katalin Komlosi: http://orcid.org/0000-0002-6076-9992
Cristina Glocker: https://orcid.org/0000-0001-5077-3034
Hao-Hsiang Hsu-Rehder: http://orcid.org/0009-0002-8924-7239
Svenja Alter: https://orcid.org/0000-0003-2233-8734
Julia Kopp: http://orcid.org/0000-0002-5122-4827
Alrun Hotz: https://orcid.org/0000-0003-2560-3951
A.D. Zimmer: https://orcid.org/0000-0002-5595-9388
Ingrid Hausser: https://orcid.org/0000-0002-1095-4962
Roger Sandhoff: https://orcid.org/0000-0003-3794-9458
Vinzenz Oji: https://orcid.org/0000-0003-1380-4828
Judith Fischer: https://orcid.org/0000-0002-8580-8118

CONFLICT OF INTEREST

The authors state no conflict of interest.

ACKNOWLEDGMENTS

We wish to thank the family for their cooperation and consent to the publication. We would also like to thank the team of the molecular genetic laboratory of the Institute of Human Genetics (Freiburg, Germany) for technical assistance in the molecular genetic diagnostics.

AUTHOR CONTRIBUTIONS

Conceptualization: JF; Data Curation: JF, CG, H-HH-R, JK, SA, ADZ, IH, RS; Formal Analysis: JF, CG, ADZ, IH, RS; Funding Acquisition: JF; Investigation: JF, KK, VO, JK, CG, H-HH-R; Methodology: JK, SA, ADZ, IH, RS; Project Administration: JF, KK; Resources: JF; Software: ADZ; Supervision: JF, SA; Validation: JF, CG, SA, ADZ; Visualization: CG, H-HH-R, AH, IH; Writing - Original Draft Preparation: JF, KK, CG; Writing - Review and Editing: JF, KK, CG, SA, IH, RS, VO

SUPPLEMENTARY MATERIAL

Supplementary material is linked to the online version of the paper at www.jidonline.org, and at https://doi.org/10.1016/j.jid.2024.03.041.

REFERENCES

Akiyama M. Corneocyte lipid envelope (CLE), the key structure for skin barrier function and ichthyosis pathogenesis. J Dermatol Sci 2017;88:3–9.

Amin N, Belonogova NM, Jovanova O, Brouwer RW, van Rooij JG, van den Hout MC, et al. Nonsynonymous variation in NKPD1 increases depressive symptoms in European populations. Biol Psychiatry 2017;81:702–7.

Aravind L, Iyer LM, Leipe DD, Koonin EV. A novel family of P-loop NTPases with an unusual phyletic distribution and transmembrane segments inserted within the NTPase domain. Genome Biol 2004;5:R30.

Balasingam N, Brandon HE, Ross JA, Wieden HJ, Thakor N. Cellular roles of the human Obg-like ATPase 1 (hOLA1) and its YchF homologs. Biochem Cell Biol 2020;98:1–11.

Boyden LM, Zhou J, Hu R, Zaki T, Loring E, Scott J, et al. Mutations in ASPRV1 cause dominantly inherited ichthyosis. Am J Hum Genet 2020;107:158–63.

Candi E, Schmidt R, Melino G. The cornified envelope: a model of cell death in the skin. Nat Rev Mol Cell Biol 2005;6:328–40.

Fischer J, Bourrat E. Genetics of inherited ichthyoses and related diseases. Acta Derm Venereol 2020;100:adv00096.

Frost P, van Scott EJ. Ichthyosiform dermatoses. Classification based on anatomic and biometric observations. Arch Dermatol 1966;94:113–26.

Genecards. *NKPD1* Gene - NTPase KAP Family P-Loop Domain Containing 1. https://www.genecards.org/cgi-bin/carddisp.pl?gene=NKPD1; 2023. (accessed January 14, 2024).

Heinz L, Kim GJ, Marrakchi S, Christiansen J, Turki H, Rauschendorf MA, et al. Mutations in SULT2B1 cause autosomal-recessive congenital ichthyosis in humans. Am J Hum Genet 2017;100:926–39.

Hotz A, Oji V, Bourrat E, Jonca N, Mazereeuw-Hautier J, Betz RC, et al. Expanding the clinical and genetic spectrum of KRT1, KRT2 and KRT10 mutations in keratinopathic ichthyosis. Acta Derm Venereol 2016;96:473–8.

Jennemann R, Rabionet M, Gorgas K, Epstein S, Dalpke A, Rothermel U, et al. Loss of ceramide synthase 3 causes lethal skin barrier disruption. Hum Mol Genet 2012;21:586–608.

Knöbel M, O'Toole EA, Smith FJ. Keratins and skin disease. Cell Tissue Res 2015;360:583–9.

Kolde G, Happle R, Traupe H. Autosomal-dominant lamellar ichthyosis: ultrastructural characteristics of a new type of congenital ichthyosis. Arch Dermatol Res 1985;278:1–5.

Lander E, Kruglyak L. Genetic dissection of complex traits: guidelines for interpreting and reporting linkage results. Nat Genet 1995;11:241–7.

Marekov LN, Steinert PM. Ceramides are bound to structural proteins of the human foreskin epidermal cornified cell envelope. J Biol Chem 1998;273:17763–70.

Melnik B, Küster W, Hollmann J, Plewig G, Traupe H. Autosomal dominant lamellar ichthyosis exhibits an abnormal scale lipid pattern. Clin Genet 1989;35:152–6.

Oji V, Tadini G, Akiyama M, Blanchet Bardon C, Bodemer C, Bourrat E, et al. Revised nomenclature and classification of inherited ichthyoses: results of the First ichthyosis Consensus Conference in Sorèze 2009. J Am Acad Dermatol 2010;63:607–41.

Ott J. Major strengths and weaknesses of the lod score method. Adv Genet 2001;42:125–32.

Pilz R, Opálka L, Majcher A, Grimm E, Van Maldergem L, Mihalceanu S, et al. Formation of keto-type ceramides in palmoplantar keratoderma based on biallelic KDSR mutations in patients. Hum Mol Genet 2022;31:1105–14.

Schimek K, Hsu HH, Boehme M, Kornet JJ, Marx U, Lauster R, et al. Bioengineering of a full-thickness skin equivalent in a 96-well insert format for substance permeation studies and Organ-On-A-chip applications. Bioengineering (Basel) 2018;5:43.

Scott R, Neeley C, Newman R, Granchell J. Establishing Human Skin Model Tissue Using Thermo Scientific NUNC Cell Culture Inserts and Carrier Plates. https://assets.thermofisher.com; 2016. (accessed January 15, 2024).

Stelzer G, Rosen N, Plaschkes I, Zimmerman S, Twik M, Fishilevich S, et al. The GeneCards suite: from gene data mining to disease genome sequence analyses. Curr Protoc Bioinformatics 2016;54(1.30):1–33.

The Human Protein Atlas. https://www.proteinatlas.org/; 2023. (accessed January 15, 2024).

Traupe H. The ichthyoses: a guide to clinical diagnosis, genetic counseling, and therapy. Berlin, Heidelberg: Springer; 1989.

Traupe H, Kolde G, Happle R. Autosomal dominant lamellar ichthyosis: a new skin disorder. Clin Genet 1984;26:457–61.

SUPPLEMENTARY MATERIALS AND METHODS

Whole-exome sequencing and Sanger sequencing

Because there was no confirmed genetic diagnosis until the age of 60 years in the index patient (Figure 1, III/2), a multigene panel of 66 genes associated with nonsyndromic and syndromic ichthyosis (in-house designed HaloPlex Custom Kit, Agilent Technologies) was initially performed from DNA extracted from peripheral blood. For further analysis, whole-exome sequencing of the index patient (III/2), her son (IV/4), and her affected nephew (IV/3) was performed. Target enrichment of all coding genomic regions (exome) was carried out with a Twist Human Core Exome Kit (Twist Bioscience), and sequencing was run on an Illumina platform (NextSeq500 System, Illumina) with 150 bp paired-end reads. The average sequencing depth per exome was at least 70.1x, and 95.1% of the coding regions and adjacent intronic regions (Consensus Coding Sequence ±20 bp) were covered by at least 20 reads. Variants were filtered using the following criteria: not in in-house database, not homozygous and <0.1% allele frequency in gnomAD (Genome Aggregation Database), not benign/likely benign in ClinVar, and in coding/splicing regions. Candidate causative variants were validated, and segregation analyses in affected and unaffected family members were performed by Sanger sequencing.

Isolation of primary keratinocytes and fibroblasts

The skin biopsies were washed sequentially in 70% ethanol, DMEM medium with penicillin/streptomycin (P/S), and Dulbecco's PBS (Gibco). Next, the skin was cut in small pieces and digested with 5 mg/ml Dispase (Gibco) in DMEM overnight at 4 °C to separate epidermis and dermis. The epidermis pieces were then incubated for 15 minutes in Trypsin 0.05% (PAN-Biotech) at 37 °C and then shredded with the help of tweezers. In addition, by resuspending several times, keratinocytes were detached from the epidermis. Trypsin was inactivated by addition of Dulbecco's PBS supplemented with 10% fetal bovine serum (PAN-Biotech). The suspension was thereafter centrifuged for 5 minutes at 300*g*, and the supernatant was discarded. The pellet was resuspended with EpiLife medium (Thermo Fisher Scientific) containing 1% human keratinocyte growth supplement (HKGS) (Thermo Fisher Scientific) and transferred to a cell culture dish. After 2–3 days, 1% P/S (PAN-Biotech) was added (EpiLife + HKGS + P/S). Meanwhile, the dermis pieces were let to adhered to a cell culture dish for 20 minutes before adding DMEM (Gibco) supplied with 1% P/S and 10% fetal bovine serum (PAN-Biotech). After 2 weeks of culture, the fibroblasts grew out of the dermis and were transferred into a cell culture dish.

Medium was changed 3 times per week. The cells (keratinocytes and fibroblasts) were harvested at 80% confluency and frozen with fetal calf serum (PAN-Biotech) + 10% DMSO (Carl Roth) and then stored in liquid nitrogen.

Embedding

For embedding, skin was fixed in 4% paraformaldehyde (Thermo Fisher Scientific) overnight at 4 °C. After gradual dehydration with ethanol (50%, 70%, 90%, 95%, 99%, and ROTI Histol [Carl Roth]), tissue was embedded in paraffin (ROTI Plast, Carl Roth). Sections of 8 μm thickness were cut and fixed on slides.

For cryosections, the skin was embedded in Tissue Tek (Sakura Finetek) and directly frozen at −80 °C. Sections of 8 μm thickness were cut and fixed on slides.

Immunohistochemical staining

Skin samples, 8-μm thick and embedded in paraffin, were dewaxed using ROTI Histol (Carl Roth) and hydrated with ethanol (99, 90, 70, 30%). Subsequently, after washing with water, the samples underwent retrieval in a pressure cooker at pH 6 in citrate buffer and were then blocked for 2 hours using 5% BSA (Santa Cruz Biotechnology). Anti-NKPD1 rabbit antibody (c-terminal) (Sigma-Aldrich) was diluted 1:200 in SignalStain Antibody Diluent (Cell Signaling Technology) and incubated overnight at 4 °C. Upon washing with PBS and staining with the secondary antibody SignalStain Boost IHC Detection Reagent (horseradish peroxidase, rabbit from Cell Signaling Technology) for 30 minutes, samples were incubated for 2 minutes with 30 μm SignalStain DAB Chromogen Concentrate (Cell Signaling Technology) diluted in 1 ml of SignalStain DAB Diluent (Cell Signaling Technology). Slides were thereafter stained with hematoxylin and cover slipped.

H&E staining

After dewaxing and hydration of the samples as described earlier, slides were washed with distilled water and stained with hematoxylin (H&E fast staining solution 1, Carl Roth) for 6 minutes, dipped in 0.1% hydrochloric acid, and rinsed with tap water. After staining with eosin (H&E fast staining solution 2, Carl Roth) for 2 minutes, samples were dehydrated with ethanol (70, 90, and 99%) and covered up with ROTI Histokitt (Carl Roth).

Immunofluorescence staining

Tissue Tek–embedded slides were washed with PBS, incubated with autofluorescence-reducing kit reagent A (Max Block Kit, Dianova) for 20 minutes, and washed with water. After heat-induced epitope retrieval in a pressure cooker at pH 6 in citrate buffer, the slides were blocked for 2 hours with 5% BSA (Santa Cruz Biotechnology). Antibody staining was performed overnight at 4 °C. After incubation with secondary antibody, slides were treated with autofluorescence-reducing kit reagent B (Max Block Kit, Dianova) for 5 minutes, covered with mounting medium (Roti-Mount FluorCare DAPI, Carl Roth), and stored at 4 °C until imaging. Antibodies used are provided in Supplementary Table S2.

Ultrastructural analysis

The skin biopsy was fixed for at least 2 hours at room temperature in 3% glutaraldehyde solution in 0.1 M cacodylate buffer pH 7.4, cut into pieces of ca. 1 mm^3, washed in buffer, postfixed for 1 hour at 4 °C in 1% aqueous osmium tetroxide, rinsed in water, dehydrated through graded ethanol solutions, transferred into propylene oxide, and embedded in epoxy resin (glycidether 100). Semithin and ultrathin sections were cut with an ultramicrotome (Reichert Ultracut E). Semithin sections of 1 μm were stained with methylene blue. A total of 60–80 nm ultrathin sections were treated with uranyl acetate and lead citrate and examined with an electron microscope JEM 1400 equipped with a 2K TVIPS CCD Camera TemCam F216.

RNA analysis

RNA of the affected individual III/1 and a healthy donor was isolated from keratinocytes and fibroblasts kept in culture for 3 days and additionally from keratinocytes at days 0, 3, 7, and 14 of induced differentiation using the RNeasy Mini Kit using QIAshredder and column DNA digestion (Qiagen) according to the manufacturer's instructions. In addition, RNA of a healthy donor was isolated from whole blood using the PAXgene Blood RNA Kit (PreAnalytiX GmbH). cDNA was synthesized using the QuantiTect reverse transcription kit (Qiagen). PCRs were performed according to standard protocols. Primer sequences used for PCR are available on request. qPCR was performed in triplicates using SYBR Green reagents (Qiagen). Primer pairs for the amplification of *NKPD1* and the housekeeping genes *HPRT* and *ACTB* were purchased from Qiagen (QuantiTect Primer Assay). Fluorescence intensities were monitored over 45 cycles on a LightCycler 480 Instrument (Roche), and relative mRNA expression was calculated with the $2^{-\Delta\Delta Ct}$ method.

Mass spectrometric ceramide analysis

Stratum corneum tape stripping, subsequent lipid extraction, and analysis by ultraperformance liquid chromatography electrospray ionization tandem mass spectrometry using external and internal standards for sphingolipids were performed as described previously (Pilz et al, 2022) with slight modifications: in addition, C26-EOS-Cer (d18:1/ωh26:0/D9-18:1) and C26-EOS-Cer(t18:0/ωh26:0/D9-18:1) were taken to quantify esterified ceramides, and instead of C17-sphinganine and -sphingosine, the sphingoid bases D7-Sa(d18:0) and D7-So(d18:1) were used as internal standards. All these standards were obtained from Avanti Polar Lipids.

Generation of 3-dimensional skin models

Two different 3-dimensional skin models—epidermal skin equivalents and full-thickness skin equivalents—were generated using primary keratinocytes from patient III/1 and a healthy donor. The epidermal skin equivalents were established according to the protocol published by Thermo Fisher Scientific (establishing human skin tissue on Nunc Cell Culture Inserts in Carrier Plate Systems, https://assets.thermofisher.com).

Full-thickness skin equivalent generation was based on our previously published protocol (Schimek et al, 2018), which was optimized and adapted to 24-well Nunc cell culture inserts (0.4 μl pore size) (Thermo Fisher Scientific). To generate the dermis equivalent, we prepared a collagen–fibroblast mixture consisting of 79% rat tail collagen (8 mg/ml) (Corning, Amsterdam, The Netherlands), 10% 10× Hanks' Balanced Salt Solution (Gibco), 1% sodium hydroxide, and 1 M and 10% fibroblast suspension (2×10^6 cells/ml in DMEM with 10% fetal calf serum, 1% P/S, and 50 μl/ml L-ascorbic acid [Sigma-Aldrich]) added last. All steps were performed on ice to avoid premature polymerization. A total of 180 μl of the mixture was transferred to a 24-well Nunc cell culture insert, placed in the lowest culture position in the plate, and polymerized for 60 minutes at 37 °C. A total of 100 μl of keratinocyte suspension, adjusted to a concentration of 2.90×10^6 cells/ml in EpiLife medium + 1% HKGS, was then transferred onto the polymerized collagen and allowed to settle. After 30 minutes, 400 μl of medium was added to the cell culture insert, and a further 600 μl was added to the surrounding 24-well vessel. After 24 hours, the incubation medium was replaced by EpiLife medium + 1% HKGS supplemented with 1.5 mM calcium chloride. After further 24 hours, the medium on top of the full-thickness skin equivalents was removed, and the cell culture insert was raised to its highest position. For air-lift cultivation, 1.5 ml EpiLife medium + 1% HKGS and 1.5 mM calcium chloride supplemented with 50 μl/ml L-ascorbic acid and 5 ng/ml keratinocyte GF (PeptroTech) were added to the 24-well vessel (bottom). The full-thickness skin equivalents were cultured for a further 14 days in air-lift conditions, with the medium changed 3 times a week.

SUPPLEMENTARY REFERENCES

Pilz R, Opálka L, Majcher A, Grimm E, Van Maldergem L, Mihalceanu S, et al. Formation of keto-type ceramides in palmoplantar keratoderma based on biallelic KDSR mutations in patients. Hum Mol Genet 2022;31:1105–14.

Schimek K, Hsu HH, Boehme M, Kornet JJ, Marx U, Lauster R, et al. Bioengineering of a full-thickness skin equivalent in a 96-well insert format for substance permeation studies and Organ-On-A-chip applications. Bioengineering (Basel) 2018;5:43.

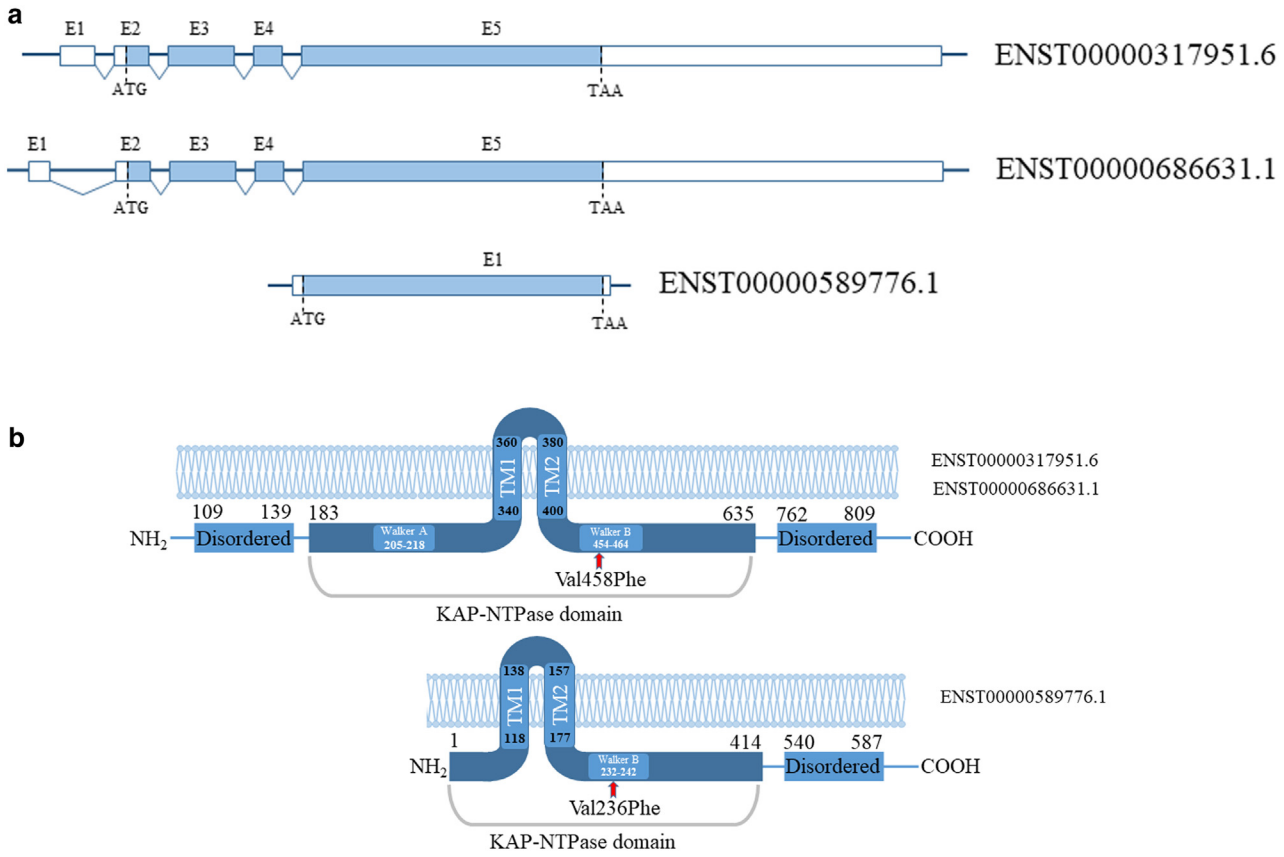

Supplementary Figure S1. Schematic representation of NKPD1. (**a**) According to the Ensemble genome browser (GRCh38.p13), *NKPD1* (*chr19:45149744-45162841)* has 3 transcripts (ENST00000686631.1, ENST00000317951.6, and ENST00000589776.1). Two of the 3 transcripts (one of 4822 bp and one of 4910 bp) consist of 5 exons encoding the same 832-amino acid protein, differing only in the 5′UTR. The third transcript of 1950 bp is encoded by only 1 exon. (**b**) Schematic representation of the NKPD1 protein according to database predictions (www.uniprot.org). Both the long and the short transcripts have at least 2 transmembrane domains. The short transcript lacks the predicted Walker A domain. The variant found in our family affects all 3 transcripts. TM, transmembrane; UTR, untranslated region.

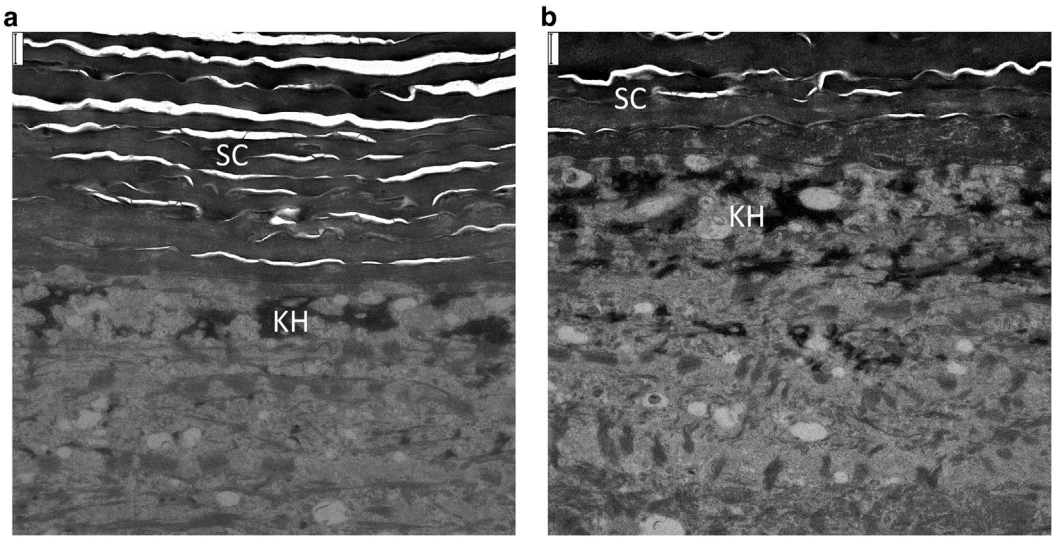

Supplementary Figure S2. Ultrastructural analysis of the skin from patient IV/3. (**a, b**). Electron microscopy showed no systematic ultrastructural aberrations of components involved in terminal differentiation or keratinization. Flat horny lamellae are homogeneous without inclusions; there are normal keratohyalin granules, lamellar bodies, and tonofilaments. Bars = 500 nm. KH, keratohyalin granule; SC, stratum corneum.

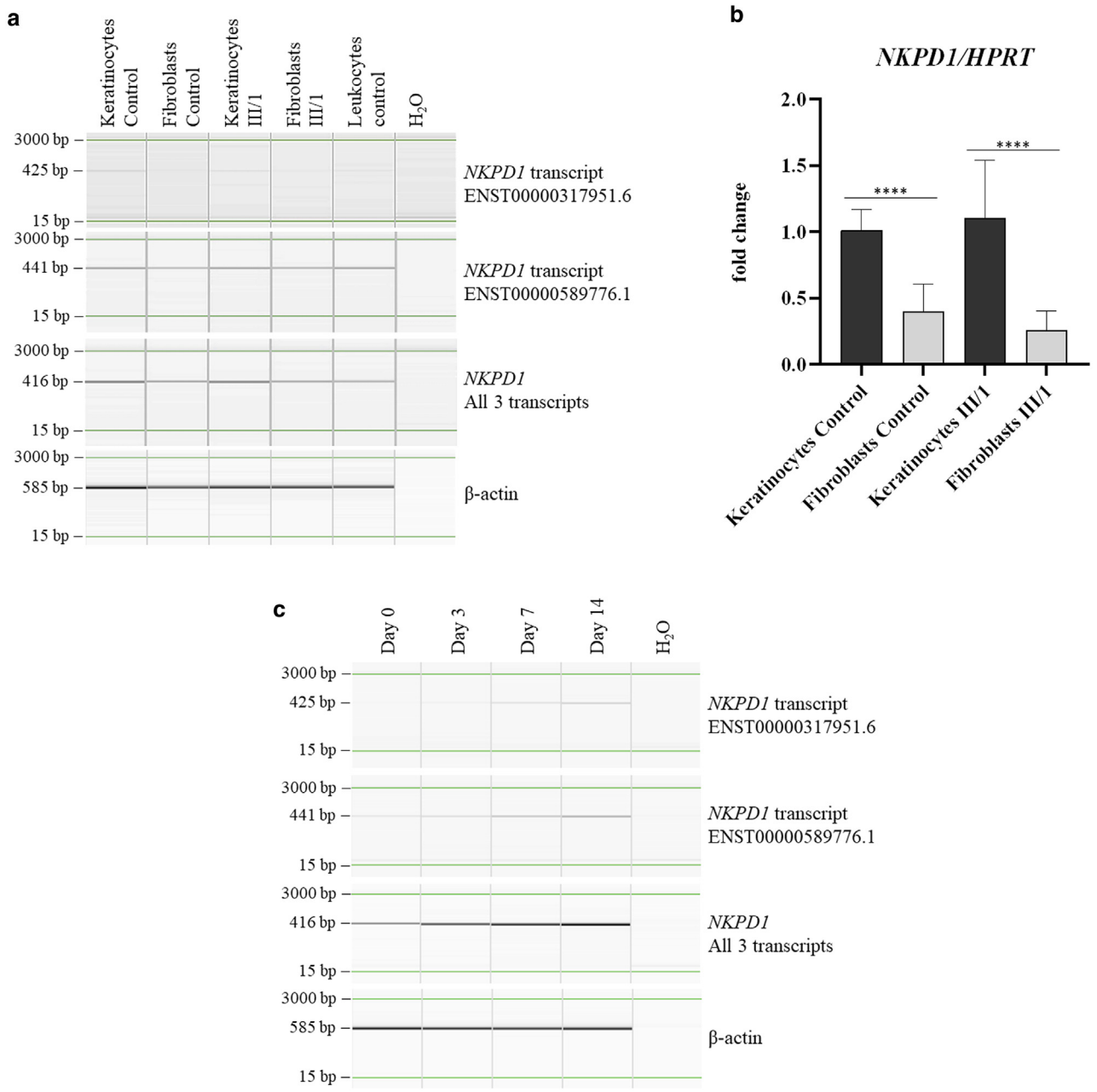

Supplementary Figure S3. *NKPD1* mRNA expression in patients' skin. (**a**) ENST00000317951.6 and ENST00000589776.1 were separately detectable by RT-PCR in both healthy control and patient keratinocytes. Expression of both transcripts was also detected in fibroblasts and leukocytes; however, resulting bands appear less intense. (**b**) *NKPD1* mRNA expression in patients' undifferentiated keratinocytes and fibroblast is comparable with *NKPD1* mRNA expression of undifferentiated keratinocytes and fibroblast of the healthy control. Data from 3 independent experiments were normalized to mean of relative expression in keratinocytes of healthy donor. (**c**) *NKPD1* mRNA expression during keratinocyte differentiation in in vitro 2D culture reached highest levels on day 14 of culture. 2D, 2-dimensional.

Supplementary Table S2. Antibodies Used in this Study

Antibodies	Dilution in PBS + BSA	Manufacturer
Anti-NKPD1 rabbit (c-terminal)	1:200	Sigma-Aldrich
Anti-glucosylceramide rabbit	1:200	Gibco
Anti-FLG rabbit	1:200	Covance
Anti-involucrin mouse	1:200	Sigma-Aldrich
Anti-cytokeratin 1/10 mouse	1:200	EMD Millipore
Anti-cytokeratin 6 rabbit	1:200	Epitomics
rabbit IgG Alexa Fluor 488	1:500	Invitrogen
rabbit IgG Alexa Fluor 594	1:500	Invitrogen
mouse IgG Alexa Fluor 488	1:500	Invitrogen
mouse IgG Alexa Fluor 594	1:500	Invitrogen